journal

J. Am. Ceram. Soc., **88** [8] 2202–2208 (2005)
DOI: 10.1111/j.1551-2916.2005.00407.x

Stress Relaxation of Compression Loaded Plasma-Sprayed 7 Wt% Y_2O_3–ZrO_2 Stand-Alone Coatings

Graeme R. Dickinson, Chris Petorak, Keith Bowman, and Rodney W. Trice†

School of Materials Engineering, Purdue University, West Lafayette, Indiana 47907

Stand-alone plasma-sprayed tubes of 7 wt% Y_2O_3–ZrO_2 made from the same starting powder but at two different sites were subject to stress-relaxation testing in axial compression at temperatures of 25°, 1000°, 1050°, 1100°, and 1200°C and at an initial stress of 10–80 MPa. A time-dependent stress response was observed for both coatings at all temperatures. For example, a 20 MPa stress applied at 1050°C relaxed to ~3 MPa in 180 min. When the same initial stress was applied at 1200°C, the coating fully relaxed in 32 min. For all experimental conditions evaluated, an initial fast stress-relaxation regime was observed (<10 min), followed by a slower second stress-relaxation regime at later times (>10 min). Coatings with higher as-sprayed densities exhibited a lengthened fast relaxation regime as compared with less dense coatings. A Maxwell model was modified in order to provide an accurate fit to the experimental stress-relaxation curves. From scanning electron microscopy experiments and mechanical data, the mechanism for stress relaxation from 25°C through 1200°C, particularly during fast relaxation, was proposed to be the formation of cracks parallel with respect to the applied load. In addition to this mechanism, stress relaxation that occurred in specimens tested at 1000°C through 1200°C was proposed to be due to partial or complete closure of cracks oriented perpendicular to the applied stress.

I. Introduction

PLASMA-SPRAYED thermal barrier coatings (TBCs) are used as protective coatings in high-temperature environments such as gas-turbine engines.[1–4] TBCs typically consist of a metallic substrate coated with an ~100 μm MCrAlY (where M stands for Ni, Co, or Fe) or PtAl bondcoat, followed by an ~200 μm topcoat with a composition of 7 wt% Y_2O_3–93 wt% ZrO_2 (YSZ). Plasma-sprayed coatings of YSZ have a layered lamellar microstructure that contains a significant volume fraction of cracks and pores, differing in both orientation and morphology, and porosity as high as 20%.[5] Lenticular-shaped interlamellar pores are oriented approximately parallel to the substrate and form due to air entrapment during rapid solidification of the molten particles.[5,6] Intralamellar cracks are oriented approximately perpendicular to the substrate and form due to thermally generated tensile stresses that occur upon cooling.[5,6] A columnar grain structure also forms within each lamella upon cooling due to the temperature gradient that develops between the cooler substrate and solidifying molten droplet.[5]

Significant morphological changes such as intralamellar crack and pore closure and loss of the columnar grain structure can occur in plasma-sprayed YSZ as a result of exposure to high temperatures. Ilavsky *et al.*[7] have related the shapes of defects in plasma-sprayed YSZ to their respective behavior at elevated temperatures. In their study, *in situ* small-angle neutron scattering (SANS) was used to monitor the decrease in the void-specific surface area of both interlamellar pores and intralamellar cracks during heating to 1400°C. It was shown that a decrease in the specific surface area of intralamellar cracks was visible after short times at 800°C, below the normal operating temperature of a gas turbine engine. These cracks were observed to be closed completely at 1000°C, while the interlamellar pores began to shrink at temperatures above 1000°C.

Thermomechanical stresses also develop within these coatings during service. Due to the low thermal conductivity of the YSZ as compared with the metallic structure, surface temperatures can increase rapidly during engine start-up, resulting in a large thermal gradient in the TBC. This gradient results in thermal expansion differences through the thickness of the TBC, and due to the cooler and stiffer metallic substrate ($E \sim 200$ GPa for Ni-based superalloys), can result in an effective compressive stress in the YSZ.[8] Kokini *et al.*[9] have found that the compressive stress in a 1 mm thick YSZ on a steel substrate under high heat flux laser heating reached 112 MPa after only 1.1 s. At ~800°C, complex time-dependent deformation consisting of sintering and compaction causes densification of the coating; it has been proposed that the time-dependent deformation observed in these coatings is a result of stress-induced mechanical sliding, as well as a thermal- and stress-activated diffusion process.[10] Sintering of the coating is enhanced by the thermally generated compressive stress state; this stress will decrease or "relax" with coating densification. For example, the maximum compressive stress of 112 MPa previously cited[9] decreased under thermal load to a value of ~30 MPa via stress-relaxation mechanisms.

Upon cooling, the TBC system will contract. While the substrate will return to its original dimensions, the densification of the topcoat during service will cause residual tensile stress to develop in the coating, as high as 124 MPa, as reported by Kokini *et al.*[9] The porous ceramic microstructure will not sustain this tensile stress, resulting in crack initiation and propagation through the thickness of the YSZ[9] proportional to the amount of coating relaxation. Thus, the goal of the current work is to investigate the stress-relaxation behavior of YSZ coatings by simulating the stress state developed during engine start-up. In the present work, this is simulated using stress-relaxation testing at elevated temperatures on stand-alone tubes of YSZ loaded in compression. Despite the fact that stress relaxation has similarities to the loading conditions experienced in service, it is still important to realize that it is a simplification of the stress state actually experienced by the coating. A uniaxial compressive stress-relaxation test will produce a uniaxial compressive stress, while a coating in service will experience biaxial compressive stresses. Regardless, the stress-relaxation behavior of a coating in service has a direct impact on crack growth, coating life, and failure of that coating. The amount that the compressive stresses decrease over time due to coating relaxation will determine the amount of tensile stress a coating will experience upon cooling.[11,12] This stress-relaxation behavior will therefore dictate the

G. Scherer—contributing editor

Manuscript No. 20179. Received July 29, 2004; approved March 4, 2005.
This work was supported by the National Science Foundation through DMR-0134286 and HRD-0120794.
Based in part on the thesis submitted by G. Dickinson for the M.S. Degree in Materials Engineering, Purdue University, West Lafayette, Indiana, 2004.
The plasma arc spraying work at Site 2 was performed by the Materials Preparation Center at the Ames Laboratory, which is supported by U.S. Department of Energy, Office of Science through Iowa State University under Contract No. W-7405-ENG-82.
†Author to whom correspondence should be addressed. e-mail: rtrice@purdue.edu

severity and density of cracking due to tensile stresses upon cooling.

II. Experimental Procedure

(1) Sample Fabrication and Physical Testing

Cylindrical stand-alone coatings were prepared using a yttria-stabilized zirconia powder (H.C. Starck, Amperit 825.0 powder, Newton, MA) with a composition of 7 wt.% Y_2O_3–93 wt.% ZrO_2 (YSZ), consisting of a particle size of ~22.5 μm. Coatings were produced at two different sites; the parameters used for each are listed in Table I. For Site 1 (designated as S1), stand-alone coatings were fabricated by first spraying aluminum powder (Sulzer Metco, 54NS-1, Winterthur, Switzerland) onto a 300 mm long alumina rod. Each alumina rod was 13 mm in diameter, and was rotated at a rate of 200 rpm during plasma-spray processing, with air cooling through the center of the tube to minimize its heating. The plasma-spray gun rastered along the length of the rod, depositing a thin ~200 μm layer of aluminum, which was subsequently lightly sanded and cleaned in acetone. Next, an ~300 μm layer of YSZ was sprayed onto the aluminum-coated alumina substrate. For Site 2 (designated as S2) coatings, the YSZ was sprayed directly on 13 mm diameter copper rods.

Rods sprayed at either site were next sectioned into multiple ~15–20 mm long cylinders using a diamond-coated blade. The two faces of each cylinder were machined parallel using a diamond tool on a lathe. The outer diameter of each YSZ tube was measured using digital calipers with a resolution of ±10 μm. This measurement was performed before removal from the alumina substrate due to handling issues inherent to the fragile stand-alone coatings. After machining, the samples were immersed in a weak HCl solution to dissolve either the intermediate aluminum layer (S1 coatings) or the copper substrate (S2 coatings) and released the YSZ layer. Approximately 10–12 samples were produced from each plasma-sprayed rod. The height and thickness of the coatings were measured after removal from the substrate, from which the inner diameter and cross-sectional area of each sample were calculated.

Bulk density, open, closed, and total porosity were measured from coatings made at both sites using the Archimedes Method, using 6.08 g/cm^3 as the theoretical density.[13] YSZ tubes were soaked in water at least 12 h prior to measuring suspended and saturated masses.

(2) Stress-Relaxation Testing

High-temperature compression testing was performed using a servo-hydraulic load frame (MTS 810 load frame) equipped with hydraulic collet grips, an alignment fixture (MTS 609 alignment fixture), a 100 kN force transducer, SiC pushrods, and a high-temperature furnace (Applied Test Systems, Inc., Butler, PA). Strain was measured with a high-temperature extensometer (MTS 632.70H-01) with a resolution of ±1 μm. The design of the extensometer was such that an alumina pushrod extended vertically through the center of the lower SiC pushrod, through a small hole in the lower SiC compression platen, through the hollow stand-alone YSZ sample, and to the surface of the upper SiC pushrod. Strain was measured as the extensometer recorded any displacement between the stationary upper compression platen and the cantilever supporting the pushrod. The distance between the upper platen and the cantilever under an applied load was governed by the material response of the stand-alone coating between the platens.

Alignment of the load frame was adjusted prior to testing the coatings to ensure that load was distributed equally around the circumference of the sample. Alignment was achieved by elastically loading a cylindrical aluminum specimen that had four strain gauges (Vishay Measurements Group, Raleigh, NC) positioned 90° from each other on the outside surface. The alignment fixture was then adjusted until identical strain readings were obtained from the strain gauges adhered to the aluminum sample.

Stress-relaxation tests were performed on the stand-alone YSZ samples at temperatures ranging from 1000° to 1200°C, and compressive stresses ranging from 10 to 80 MPa. Each sample was heated to the desired temperature at a rate of 10°C/min under no applied load. After the target temperature was reached and stabilized for 15 min, the test was initiated by monotonically increasing the stress applied to the YSZ tube at a rate of 20 N/s to a pre-determined initial stress. Once the initial stress was reached, the control system was rapidly changed from force to strain feedback, and the strain was held constant for 3 h. The material response was measured by observing the stress reduction with time. The noise in the load signal represents ±1 MPa uncertainty. This uncertainty value, in part, was determined by hanging weights from the load cell; the uncertainty in the load cell measurement was within ±1.5 N for loads from 0 to 90 N. Replicate testing of coatings made at Site 2 were used to establish variability in sample behavior as a function of test temperature and stress. Thermal expansion of the YSZ tubes and the load frame did not influence the material response, as no load was applied during heating or during the 15-min stabilization period. Inspection of samples after testing to stresses as high as 80 MPa shows no evidence of barreling.

The modulus values of YSZ S1 coatings tested at initial stress levels of 10 and 20 MPa at 1000°C were measured during stress-relaxation tests to evaluate the change in the elastic properties as a function of time relaxed. Modulus measurements were made by unloading YSZ tubes at specific time intervals (2, 5, 10, 60, and 180 min) during a stress-relaxation test, followed immediately by reloading to the strain level held constant throughout the test. The initial linear region of the stress-strain response was used to calculate modulus, and the compliance of the load frame was taken into account.

Table I. Comparison of Spray Parameters Used to Prepare Coatings at Site 1 (S1) and Site 2 (S2)

Parameters	S1 coating†	S2 coating‡
Power (kW)	35	37
Stand-off Distance (cm)	6	10
Arc gas rate (slm)	32 (Ar)	25 (Ar)
Aux gas rate (slm)	8 (H)	21 (He)
Powder carrier gas rate (slm)	5 (Ar)	6 (Ar)
Powder feed rate (rpm)	3	1.5

†S1 coatings were made at Northwestern University and sprayed with an A-3000 Plasma Technik control system (Siegen, Germany) equipped with an F4 gun mounted on an ASEA Brown and Boveri IRB 2000 robot. The injector angle (angle between the powder injector and plasma plume) was 30°C and the offset of the injector was 8 mm.[22] ‡S2 coatings were made at Ames National Laboratory with a Praxair SG-100 gun mounted to a 2-way stage.

(3) Stress-Relaxation Modeling

A Maxwell element, consisting of an elastic spring and viscous dashpot in series, is often used to model the stress-relaxation behavior of polymeric materials.[14–17] For the case where there are multiple relaxation phenomena, individual Maxwell elements are arranged in parallel to better fit the experimental data. In general, the experimental data can be approximated by a series of Maxwell elements arranged in parallel. This is given by

$$\sigma(t) = \sigma_0 \sum_{k=1}^{n} w_k \exp\left(-\frac{t}{\tau_k}\right) \quad (1)$$

$$\sum_{k=1}^{n} w_k = 1 \quad (2)$$

where σ_0 is the initial stress, n is the number of Maxwell elements in parallel, w_k is a weighting factor that is summed to unity, and t is the time. The time constant for each Maxwell

element, τ_k, can be further defined as:

$$\tau_k = \frac{\eta_k}{E_k} \tag{3}$$

where η_k is the viscosity of the dashpot and E_k is the modulus of the spring for each Maxwell element.

The experimental data from the current study did not fit a model that included only a single Maxwell element (i.e., $n = 1$) because at least two relaxation regimes were observed. For this case, a modified model consisting of either 2 or 3 Maxwell elements in parallel was used to fit the data. The 2-element Maxwell model is analogous to mathematically adding two separate stress-relaxation behaviors (fast and slow relaxation) at each time increment, yielding one stress-relaxation curve. For the case where relaxation did not occur within the time frame of the experiment, three Maxwell elements were required to fit the data.

Individual τ_k and w_k were fit to a given set of experimental data using a least-squares curve fitting method by minimizing R as defined in the following equation:

$$R = \sum_{t=0}^{t=t_f} \sqrt{\left| [\sigma_{exp}(t)]^2 - [\sigma_{mod}(t)]^2 \right|} \tag{4}$$

where $\sigma_{exp}(t)$ and $\sigma_{mod}(t)$ represent stress values obtained experimentally and from numerical modeling, respectively, from the start of the test ($t = 0$) until the end of the test ($t = t_f$). The R value has no physical meaning, but is minimized to provide the best fit of the model to the experimental data. Stress values were squared to give higher stress values greater weight in determining a proper fit. The square root of this difference for each time step is summed over the complete test time, yielding an R value. This value can be minimized by iteratively varying τ_k and w_k, and thereby providing the best fit of the model to the experimental stress-relaxation data. For samples tested at stresses greater than 20 MPa, the least-squares fit approach was applied first to the initial relaxation regime data to determine τ_1, followed by application of this approach to the entire data set. This was necessary to sufficiently weight the rapid relaxation observed during the initial regime where the number of data points recorded was greatly exceeded by those in the slow relaxation regime.

III. Results and Discussion

(1) Physical Properties of YSZ Coatings

The average stand-alone tube thickness, density, and porosity of plasma-sprayed coatings made at S1 and S2 are presented in Table II. S1 and S2 coating thicknesses ranged from an average of 360 to 551 μm, respectively. Coatings taken from the center portion of the rod were generally thicker than those taken from end positions. S2 coatings were more dense (and therefore less porous) than S1 coatings. Sample heights for both coatings were ~17 mm.

(2) Stress-Relaxation Response of Compression-Loaded YSZ Coatings

(A) Effect of Temperature and Density on Stress-Relaxation Response: Representative experimental stress responses for as-sprayed YSZ S1 coatings heated to 1000° and 1100°C with an initial compressive stress of 20 MPa are presented in Fig. 1. There is some uncertainty in the actual stress measured, as evident by the width of the experimental load data. From our observations and experiences testing these coatings, this error is estimated to be ±1 MPa. Complete relaxation of the initial stress at 1100°C was observed (i.e., the stress in the coating relaxed to within the measurement error of 1 MPa), while the YSZ coating tested at 1000°C did not relax fully within the 180 min test. The experimental data from each sample tested at elevated temperatures exhibited at least two stress-relaxation regimes. At early times (~0–10 min), a fast stress-relaxation regime was observed, followed by a slower relaxation regime at later times. The curve fit of stress vs. time for a 2-element Maxwell model (using Eq. (1)) is plotted in Fig. 1 along with the experimental data for a YSZ tube under an initial compressive stress of 20 MPa at 1100°C; good agreement was observed between the experimental data and the fit of the 2-element model. When complete relaxation was not observed within the time frame of the test, as shown in Fig. 1 for the experimental data at 1000°C, a 3-element Maxwell model was required to fit the experimental data.

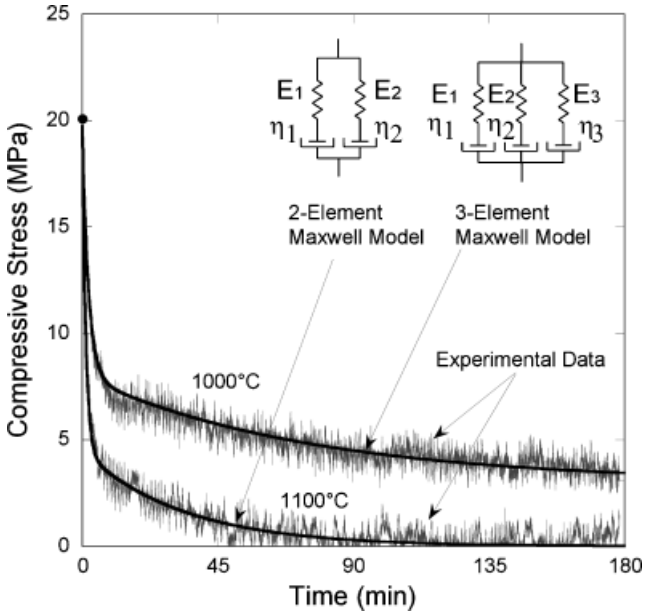

Fig. 1. Plot of experimental data for YSZ S1 coatings relaxed from 20 MPa at 1000°C and 1100°C. A 2-element Maxwell model fit the experimental results for the data obtained at 1100°C while a 3-element Maxell model fit the 1000°C data.

For clarity, Fig. 2 shows only the average modeled stress-relaxation behavior of YSZ S2 tubes at an initial stress of 20 MPa for test temperatures of 25°, 1050°, 1100°, and 1200°C. Each temperature-dependent response represents the averaged modeled stress relaxation behavior for three samples at each temperature. The compressive stress axis was plotted on a log scale to further accentuate the slow and fast relaxation behavior; the lower threshold for the plot was set at 1 MPa, the resolution of the experimental results. In the current work, S2 coatings tested at 25°C relaxed ~4 MPa under the initial 20 MPa stress during the 3 h test. Relaxation of plasma-sprayed YSZ coatings at 25°C was also observed by Rejda *et al.*[18]

As the test temperature was increased, the magnitude of stress relaxed during the fast relaxation regime also increased. For example, it varied from 8.8±0.3 to 13±0.0 MPa at 1050° and 1200°C, respectively. The fact that the magnitude of relaxed stress increased, as compared with the room-temperature sample, suggests that elevated temperatures thermally activate relaxation mechanisms.

Figure 3 compares the stress-relaxation behavior of YSZ S1 and S2 coatings at 1050°C and 1200°C. At 1050°C, the less dense

Table II. Average Physical Properties of the As-Sprayed Stand-Alone Coatings Made at Site 1 and Site 2

Property	S1 coating properties	S2 coating properties
Tube thickness (μm)	360±41	551±25
Bulk density (g/cm^3)	5.0±0.3	5.5±0.1
Open porosity (%)	10.3±3.3	2.2±1.3
Closed porosity (%)	7.0±5.2	7.2±2.3
Total porosity (%)	17.3±5.1	9.4±1.9

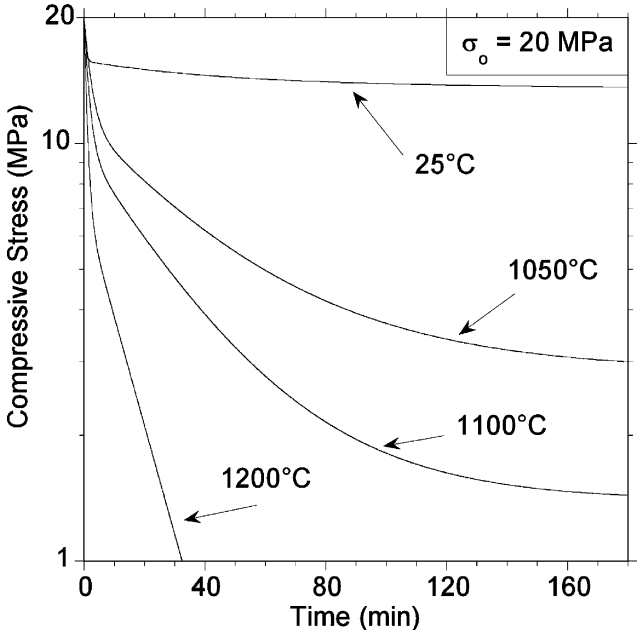

Fig. 2. Plot of the average fit of 2-element or 3-element Maxwell models as a function of test temperature for YSZ S2 coatings. A 2-element Maxwell model was used to fit data at 1200°C; a 3-element Maxwell model was used to fit data at 25°, 1050°, and 1100°C because samples tested at these temperatures did not fully relax within the 180 min test. The initial stress was 20 MPa for all samples represented in this figure.

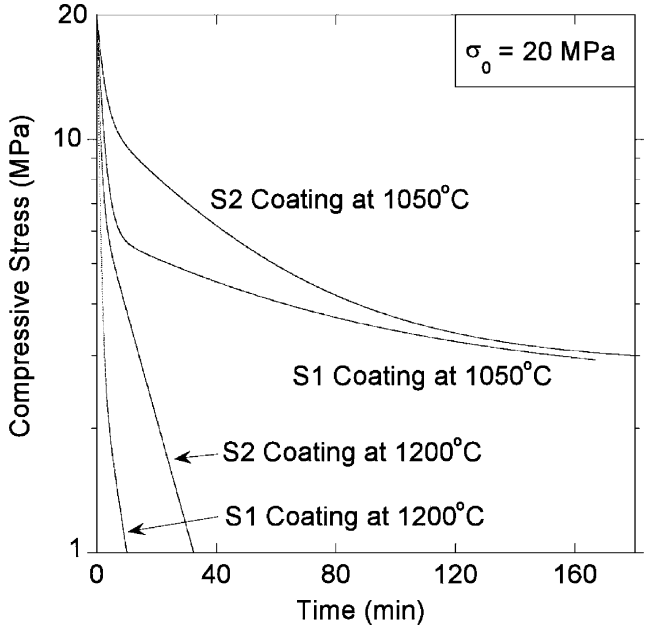

Fig. 3. Comparison of the modeled stress-relaxation response of YSZ S1 and S2 coatings when relaxed from 20 MPa at 1050° and 1200°C. The bulk densities of YSZ S1 and S2 coatings were 5.0 ± 0.3 and 5.5 ± 0.1 g/cm^3, respectively.

YSZ S1 coating demonstrates a faster initial relaxation, followed by a slower secondary relaxation, as compared with the denser YSZ S2 coating. At 1200°C, the YSZ S1 coating was observed to relax completely in 10 min as compared with the denser YSZ S2 coating, which relaxed in 32 min. Thus, it appears that the density strongly influences the relaxation behavior of plasma-sprayed YSZ coatings.

Table III shows the fitting parameters for both YSZ S1 and S2 coatings relaxed from 20 MPa. For coatings sprayed at either site, the magnitude of the initial fast relaxation stress, given by $w_1\sigma_0$, increased as the test temperature was increased. For example, the S2 coatings relaxed 8.8 ± 0.3 and 13 ± 0 MPa when tested at 1050° and 1200°C, respectively. The magnitude of relaxation observed during slow relaxation, assumed to be $w_2\sigma_0 + w_3\sigma_0$, was less than $w_1\sigma_0$ for the S1 coatings. For YSZ S2 coatings, the magnitude of stress relaxation during slow relaxation was approximately equal to $w_1\sigma_0$ for coatings that did not relax fully during the 3 h test.

The time constants that mathematically describe the initial fast relaxation, given by τ_1, and secondary slower relaxation, given by τ_2 and τ_3, were observed to decrease with increasing temperature for each coating type. That the time constants decrease with increasing temperature shows quantitatively that stress relaxation is accelerated by elevated temperature. At each test temperature, it was also observed for each coating type that fully relaxed within the 3 h test that τ_2 was greater than τ_1 by at least one order of magnitude. At 1200°C, for example, τ_1 and τ_2 were 62 ± 8 and 1000 ± 265 s, respectively, for the YSZ S2 coatings. Thus, the secondary relaxation occurred much more slowly than the initial relaxation event. For the case of coatings that did not fully relax within the 3 h test, it was observed that $\tau_3 > \tau_2 > \tau_1$. τ_3 was observed to be several orders of magnitude greater than τ_2, an indication that full relaxation of the specimen will take an extended amount of time.

A comparison of the fitting parameters in Table III indicates a difference between the stress-relaxation response of the YSZ S1 and S2 coatings that appears to be due to density differences (see Table II). For example, YSZ S2 coatings relaxed 10.3 ± 0.6 MPa at 1100°C as compared with the YSZ S1 coating that relaxed 16 MPa. At all temperatures, the fast relaxation time constants, given by τ_1, were observed to increase for the denser YSZ S2 coatings as compared with YSZ S1 coatings. τ_2 values for the YSZ S2 coatings were of similar magnitude to τ_2 values for the YSZ S1 coatings.

(B) Effect of Initial Stress on Stress-Relaxation Response: The modeled stress-relaxation response as a function of initial stress at 1100°C for YSZ S2 coatings is presented in Fig. 4(a). Samples tested at 20, 60, and 80 MPa initial stress levels did not fully relax at 1100°C within 180 min. The fitting parameters for the data presented in Fig. 4(a) are presented in Table IV. It is noteworthy that τ_1, τ_2, and τ_3 values are essentially identical, independent of the starting stress. Figure 4(b) is an isochronal plot of the data in Fig. 4(a); the material demonstrates linear viscoelastic stress-relaxation behavior for the testing parameters analyzed.

(C) Effect of Stress Relaxation on Modulus: The evolution of the YSZ S1 coating modulus during a stress-relaxation

Table III. Fitting Parameters of As-Sprayed Coatings Relaxed from 20 MPa as a Function of Temperature

Temp. (°C)	Coating	$w_1\sigma_0$ (MPa)	τ_1 (*s*)	$w_2\sigma_0$ (MPa)	τ_2 (*s*)	$w_3\sigma_0$ (MPa)	τ_3 (*s*)
1000	S1	12.0	125	5.0	4500	3.0	1×10^{14}
1050	S1	14.0	123	3.0	3800	3.0	1×10^{5}
1100	S1	16.0	93	4.0	2200	0	0
1200	S1	17.0	50	3.0	549	0	0
1050	S2	8.8 ± 0.3	143 ± 3	8.3 ± 0.6	2600 ± 391	2.8 ± 0.3	$1 \times 10^{6} \pm 0$
1100	S2	10.3 ± 0.6	102 ± 6	8.3 ± 1.2	2000 ± 250	1.3 ± 0	$1 \times 10^{8} \pm 0$
1200	S2	13 ± 0	62 ± 8	7 ± 0	1000 ± 265	0	0

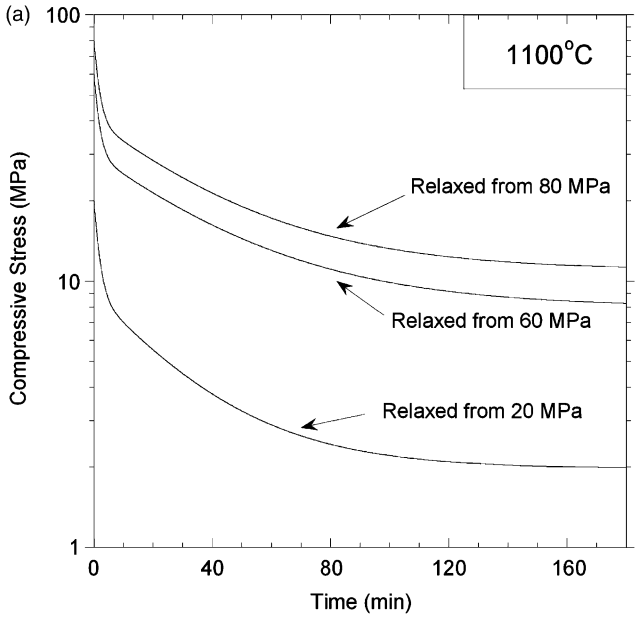

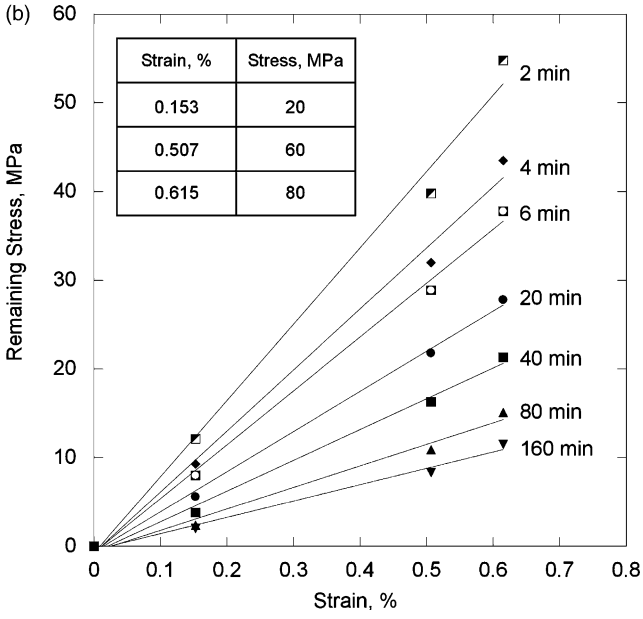

Fig. 4. (a) Plot of the fit of 3-element Maxwell models as a function of initial stress level at 1100°C for YSZ S2 coatings and (b) corresponding isochronal plot of remaining stress versus constant strain in each of the samples.

test at 1000°C for initial stress levels of 10 and 20 MPa is presented in Fig. 5. Modulus values were initially < 5 GPa, but increased to values just above 20 GPa for samples relaxed from initial applied stress levels of 10 and 20 MPa. Most of the increase in modulus was observed during the fast relaxation regime. The average difference in modulus observed between the samples tested at 10 and 20 MPa was ~1.3 GPa, showing that the change in modulus during stress relaxation was not a strong function of initial stress within the levels tested.

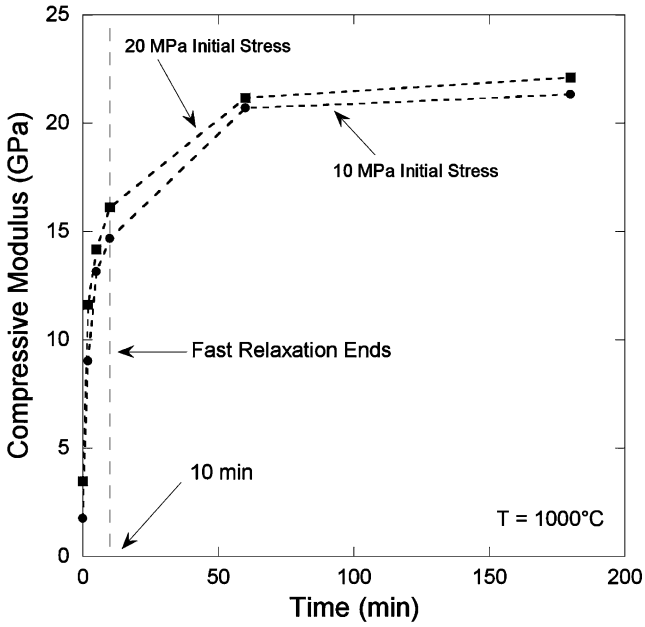

Fig. 5. Plot of modulus as a function of time at 1000°C for three initial stress levels in YSZ S1 coatings. Note that lines joining the data points have been added to guide the eye.

(3) SEM Analysis of YSZ Coatings

The top surfaces of as-sprayed, heat-treated (3 h at 1100°C), and stress-relaxed (from a 60 MPa initial stress, 3 h at 1100°C) standalone YSZ S2 coatings were analyzed using SEM. The as-sprayed coating exhibited extensive intralamellar cracking in all orientations as shown in Fig. 6(a). As indicated in the micrograph, it appears that some of the microcracks are open wider than others (i.e., coarse microcracks), while some of them appear to be much finer. Figure 6(b) shows the top surface of the YSZ coating that was heat treated for 3 h at 1100°C. Intralamellar cracking was observed in all orientations in this sample; however, there is some evidence that the smaller microcracks in all orientations have partially or completely closed, consistent with observations by prior work.[7] An SEM micrograph of a coating stress relaxed from 60 MPa at 1100°C after 3 h is presented in Fig. 6(c); in some areas, it appears that fine microcracks oriented perpendicular to the applied load have completely disappeared. However, it is very difficult to quantify any of the changes in these micrographs using SEM techniques; a technique that would take into account a larger volume (like SANS) would be particularly beneficial to delineate crack closure.

IV. Discussion

(A) Mechanism of Stress Relaxation at 25°C: The stress-relaxation behavior at 25°C (see Fig. 2) cannot be attributed to any thermally activated mechanism within the YSZ as the temperature is too low. In a prior study, acoustic emission sensors attached to a plasma-sprayed alumina tube continued to detect the formation of microcracks after the peak stress was reached.[19] The orientation of these new cracks with respect to

Table IV. Fitting Parameters of As-Sprayed Coatings Tested at 1100°C as a Function of Initial Stress

Stress (MPa)	Coating	$w_1\sigma_0$ (MPa)	τ_1 (*s*)	$w_2\sigma_0$ (MPa)	τ_2 (*s*)	$w_3\sigma_0$ (MPa)	τ_3 (*s*)
20	S2	10.3±0.6	102±6	8.3±1.2	2000±250	1.3±0	$1 \times 10^8 \pm 0$
60	S2	30	98	22	2450	8	1×10^8
80	S2	40	102	29	2350	11	1×10^8

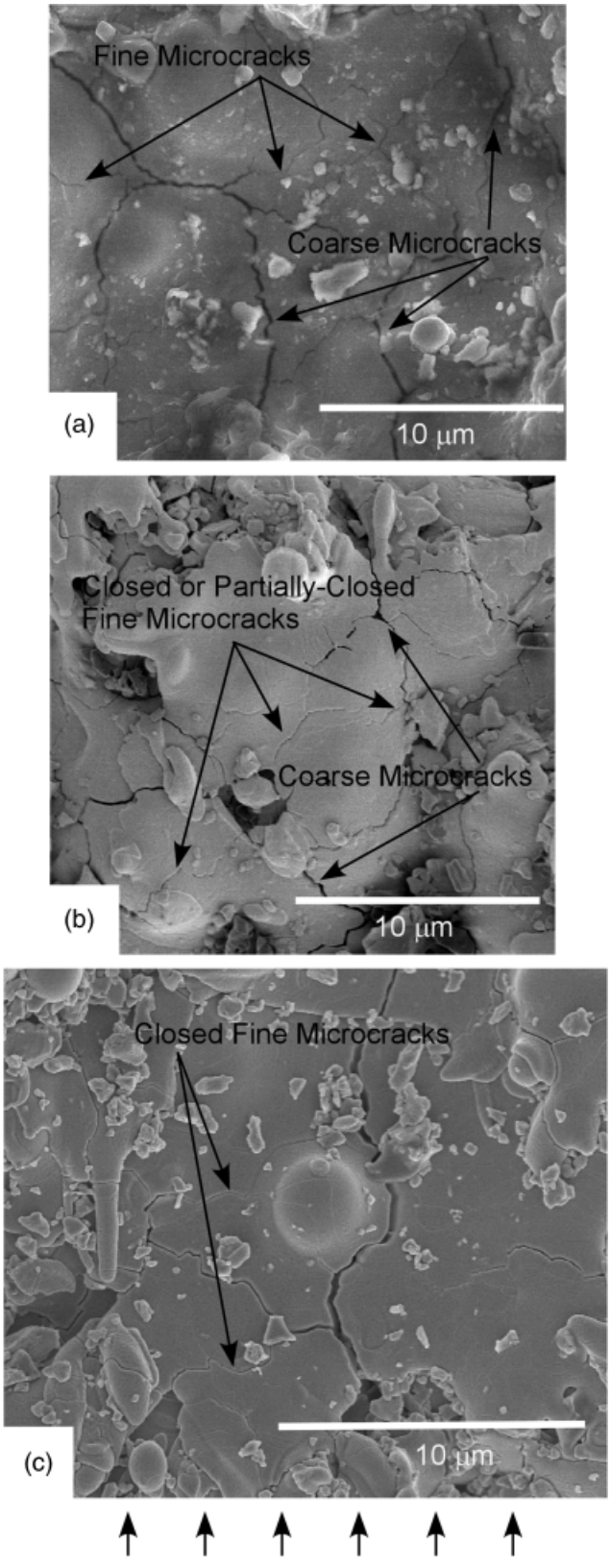

Fig. 6. SEM micrographs of the top surface of YSZ S2 coatings (a) in the as-sprayed condition, (b) after heat treatment for 3 h at 1100°C, and (c) after a 3 h stress-relaxation test (initial stress of 60 MPa) at 1100°C.

the loading direction was directly observed by Levin *et al.* [20] in plasma-sprayed YSZ, where new microcracks were observed to form parallel to the applied stress. Therefore, it is proposed that the mechanism responsible for stress relaxation at 25°C is the formation of microcracks and the concomitant reduction in strain energy stored in the sample.

(B) Mechanism of Stress Relaxation at Elevated Temperatures: The mechanism for stress relaxation at 25°C, i.e., the formation of new microcracks oriented parallel to the applied load, likely contributes at least some of the stress relaxation observed at elevated temperatures. However, the stress relaxation data presented in Figs. 1–4 clearly show that significantly more relaxation is occurring at test temperatures of 1000°C and beyond, by what can reasonably be assumed to be a thermally activated process.

It has been previously shown[19,20] that cracks oriented perpendicular to a uniaxial load in plasma-sprayed coatings will partially close at 25°C; these cracks will open up again upon unloading, as detected in tests on plasma-sprayed alumina coatings by acoustic emission sensors.[19] However, at elevated temperatures, when these cracks are partially closed by a mechanical load, crack tips and adjacent surfaces in contact would be expected to close by sintering.[21] As cracks oriented perpendicular to the applied load are preferentially closed, these would be expected to sinter first due to stress-enhanced sintering. This is also consistent with the modulus measurements presented in Fig. 5, where the increase in modulus after time at 1000°C can be attributed to a larger fraction of the load actually being carried by the YSZ coating. The increased amount of stress relaxation at temperatures equal to or greater than 1000°C can be explained by the closure and sintering of cracks. As the test temperature was increased, more complete relaxation was observed as evidenced by the reduction in τ_1 observed in Table III. It is certainly plausible that the kinetics of the sintering process would increase as temperature increased.

V. Conclusions

Uniaxial compression stress-relaxation testing was performed on stand-alone plasma-sprayed tubes of 7 wt% Y_2O_3–ZrO_2 with different densities at 1000°, 1050°, 1100°, and 1200°C, and stresses ranging from 10 through 80 MPa. The duration of the test was held constant at 3 h. For all temperatures and stresses investigated, time-dependent stress behavior was observed. All YSZ coatings demonstrated an initial fast stress-relaxation regime, typically within the first 10 min of the test, followed by a slower stress-relaxation regime at later times. A Maxwell model, generally used to model the stress-relaxation behavior of polymeric materials, was modified by adding additional Maxwell elements in parallel in order to provide an accurate fit to the experimental stress-relaxation curves. Using scanning electron microscopy and observations from the mechanical data, the mechanism for stress relaxation at all test temperatures, particularly during fast relaxation, was proposed to be the formation of cracks parallel to the applied load. In addition to this mechanism, stress relaxation at elevated temperatures was attributed to partial or complete closure of cracks oriented perpendicular to the applied stress.

References

[1]R. A. Miller, "Current Status of Thermal Barrier Coatings—An Overview," *Surf. Coat. Tech.*, **30**, 1–11 (1987).
[2]R. A. Miller, "Thermal Barrier Coatings for Aircraft Engines–History and Directions," *J. Therm. Spray Tech.*, **6** [1] 35–42 (1997).
[3]M. J. Stiger, N. M. Yanar, M. G. Topping, F. G. Pettit, and G. H. Meier, "Thermal Barrier Coatings for the 21st Century," *Z. Metallkd.*, **90** (1999).
[4]W. Beele, G. Marijnissen, and A. Van Lieshout, "The Evolution of Thermal Barrier Coatings—Status and Upcoming Solutions for Today's Key Issues," *Surf. Coat. Tech.*, **120**, 61–7 (1999).
[5]R. McPherson, "A Review of Microstructure and Properties of Plasma-Sprayed Ceramic Coatings," *Surf. Coat. Tech.*, **39/40**, 173–81 (1989).
[6]R. McPherson, "Relationship Between The Mechanism of Formation, Microstructure and Properties of Plasma-Sprayed Coatings," *Thin Solid Films*, **83** [3] 297–310 (1981).
[7]J. Ilavsky, G. G. Long, A. Allen, and C. Berndt, "Evolution of the Void Structure in Plasma-Sprayed YSZ Deposits During Heating," *Mater. Sci. Eng. A.*, **272**, 215–21 (1999).
[8]K Kokini and Y. R. Takeuchi, "Transient Thermal Fracture of an Interface Crack in the Presence of a Surface Crack," *J. Therm. Stress*, **17**, 63–74 (1994).

[9]K. Kokini, A. Banerjee, and T. A. Taylor, "Thermal Fracture of Interfaces in Precracked Thermal Barrier Coatings," *Mater. Sci. Eng. A*, **323**, 70–82 (2002).
[10]D. Zhu and R. A. Miller, "Determination of Creep Behavior of Thermal Barrier Coatings Under Laser Imposed High Thermal and Stress Gradient Conditions," *J. Mater. Res.*, **14** [1] (1999).
[11]K. R. Kokini, Y. R. Takeuchi, and B. D. Choiles, "Surface Thermal Cracking of Thermal Barrier Coatings Owing to Stress-Relaxation: Zirconia vs. Mullite," *Surf. Coat. Tech.*, **82**, 77–82 (1995).
[12]B. D. Choules, K. Kokini, and T. A. Taylor, "Thermal Fracture of Ceramic Thermal Barrier Coatings under High Heat Flux with Time-Dependent Behavior. Part 1. Experimental results," *Mater. Sci. Eng. A*, 296–304 (2001).
[13]J. B. Wachtman, *Mechanical Properties of Ceramics*, p. 392 Wiley, New York, 1996.
[14]R. M. Christensen, *Theory of Viscoelasticity—An Introduction*. Academic Press, New York, 1971.
[15]Y. C. Fung, *Foundations of Solid Mechanics*. Prentice-Hall, Englewood Cliffs, NJ, 1965.
[16]A. S. Krausz and H. Eyring, *Deformation Kinetics*. John Wiley & Sons, New York, 1975.
[17]N. G. McCrum, C. P. Buckley, and C. B. Bucknall, *Principles of Polymer Engineering*, 2nd edition, Oxford Science Publications, Oxford, 1997.
[18]E. F. Rejda, D. F. Socie, and T. Itoh, "Deformation Behavior of Plasma-Sprayed Thick Thermal Barrier Coatings," *Surf. Coat. Tech.*, **113**, 218–26 (1999).
[19]R. Trice, D. Prine, and K. Faber, "Deformation Mechanisms in Compression-Loaded Stand-Alone Plasma-Sprayed Alumina Coatings," *J. Am. Ceram. Soc.*, **83** [12] 3057–64 (2000).
[20]J. Levin, G. Dickinson, and R. Trice, "In-situ Observation of Crack Behavior in Plasma-Sprayed 7 wt% Yttria-Stabilized Zirconia," *J. Am Ceram. Soc.*, **87** [5] 960–2 (2004).
[21]G. Thurn, G. A. Schneider, and F. Aldinger, "High-Temperature Deformation of Plasma-Sprayed ZrO2 Thermal Barrier Coatings," *Mater. Sci. Eng. A.*, **A233**, 176–82 (1997).
[22]T. F. Bernecki and D. R. Marron, "Small-Particle Plasma-Spray Apparatus, Method and Coated Article," U.S. Patent No. 5 744 777, 1998, and U.S. Patent No. 5 858 470, 1999. □